MAS NMR Structures of Aggregated Cadmium Chlorins Reveal Molecular Control of Self-Assembly of Chlorosomal Bacteriochlorophylls

Ido de Boer,[†] Jörg Matysik,*[,†] Kees Erkelens,[†] Shin-ichi Sasaki,[‡] Tomohiro Miyatake,[‡,§] Shiki Yagai,[‡,||] Hitoshi Tamiaki,[‡] Alfred R. Holzwarth,[⊥] and Huub J. M. de Groot*[,†]

Biophysical Organic Chemistry, Leiden Institute of Chemistry, Einsteinweg 55, 2300 RA Leiden, The Netherlands, Department of Bioscience and Biotechnology, Faculty of Science and Engineering, Ritsumeikan University, Kusatsu, Shiga 525-8577, Japan, and Max-Planck-Institut für Bioanorganische Chemie,[#] Postfach 101365, D-45413 Mülheim an der Ruhr, Germany

Received: July 5, 2004; In Final Form: August 16, 2004

Magic angle spinning NMR spectroscopy has been used to investigate the self-organization of bacteriochlorophylls in chlorosomal light-harvesting antennae. Two model cadmium chlorins were studied that were uniformly ^{13}C and ^{15}N enriched in the ring moieties. The chlorin models differ from the natural BChl *c* in the central metal and the 3-, 12-, 17-, and 20-side chains. One model system has the farnesyl tail replaced by a methyl, whereas the other has a stearyl tail. The ^{113}Cd MAS NMR signals indicate a five-coordination of the Cd metal. In particular, the combined NMR data show a HO···Cd coordination, very similar to the HO···Mg coordination in the natural system. Anomalously large ^{1}H ring-current shifts of up to 10 ppm reveal a dense orderly stacking of the molecules in planar layers, for which a correlation length of at least 24 Å was defined from long-range ring-current shift calculations. In addition, our model structures confirm and validate the essential role of the [3^1R] and [3^1S] stereoisomers in the formation of the chlorosomal antennae, as tubular structures are not formed without this chirality. The 3D arrangement of the layers is revealed by intermolecular $^{13}C-^{13}C$ correlations obtained from CP^3 CHHC experiments. With the tail truncated to methyl, a microcrystalline solid is formed with favorable interactions between the planar sheets in a head-to-tail orientation. The stearyl tails lead to a considerably disordered aggregate consisting of both syn and anti layers similar to the chlorosomes, as indicated by a doubling of the N−D signal. These results reveal a balance between relatively strong local interactions and contributions to the free energy of the system associated with a longer length scale. This leads to a robust chlorosome structure, stable against thermodynamic noise, and allows for fine-tuning of the structure.

Introduction

Photosynthetic green sulfur bacteria contain extramembraneous light-harvesting antenna complexes called chlorosomes, which are ellipsoid vesicles of about 100−300 nm in length (for a review, see, e.g., ref 1). Chlorosomes contain tubular antennae consisting mostly of bacteriochlorophyll (BChl) *c* molecules (Figure 1) and BChl *d* or *e* in some bacteria, surrounded by a monolayer of lipids and some proteins. Via a BChl *a*−protein complex called a baseplate, which is a part of the chlorosomal envelope facing the cytoplasmic membrane, photonic excitations are funneled into membrane-bound photosynthetic reaction centers.[2−4] It has been shown that the structural organization of the chlorosomal antennae is reproduced by pure BChl *c* aggregated in hexane, which indicates that the self-assembly of BChl *c* is responsible for the tubular structure.[5−7]

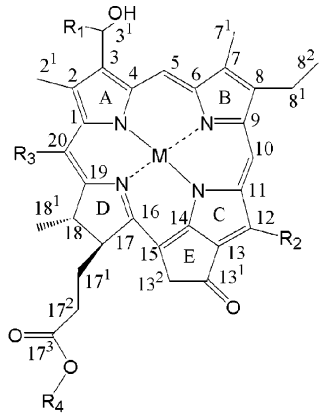

	M	R_1	R_2	R_3	R_4
BChl *c* in *C. tepidum*	Mg	Me	Et	Me	Farnesyl
Cd-Chlorin-Me (**1**)	Cd	H	Me	H	Me
Cd-Chlorin-stearyl (**2**)	Cd	H	Me	H	Stearyl

Figure 1. Chemical structure of BChl *c* and the cadmium chlorins.

Several functionalities of the building blocks, BChl *c*, *d*, or *e*, are thought to be predominant chemical factors in steering the formation of specific supramolecular assemblies in a bottom-up process. This contrasts with the emerging and top-down thermodynamic control that is generally thought to govern

* Corresponding authors. Fax: +31-71-5274603. E-mail: ssnmr@chem.leidenuniv.nl.
† Leiden Institute of Chemistry.
‡ Ritsumeikan University.
§ Present address: Department of Materials Chemistry, Faculty of Science and Technology, Ryukoku University, Otsu, Shiga 520-2194, Japan.
|| Present address: Department of Materials Science, Faculty of Engineering, Chiba University, Inage-ku, Chiba 263-8522, Japan.
⊥ Max-Planck-Institut für Bioanorganische Chemie.
Formerly known as Max-Planck-Institut für Strahlenchemie.

10.1021/jp047048+ CCC: $27.50
Published on Web 09/29/2004

mesoscopic assembly processes in most soft condensed matter systems, as these processes are, to first order, independent of the microscopic details of the molecular building blocks involved. First, a common feature in BChl *c*, *d*, or *e* aggregates is an intermolecular 13-C═O···HO···Mg structural motif. Hence, the molecular building blocks are kept together by coordination and H-bond interactions that are strong compared to, for instance, nonbonding van der Waals interactions. The C═O···HO···Mg motif can support a variety of suprastructures.[8−10] Second, chlorosomes generally contain a mixture of BChl homologues with different 8-, 12-, and 20-alkyl groups.[1] The presence of different 8- and 12-substituents does not lead to significant additional line broadening in the magic angle spinning (MAS) NMR data of the chlorosomes, which indicates that these homologues are in very similar structural environments.[7] On the other hand, molecular modeling of BChl *c* indicates that steric repulsion between the 2-Me and the 20-Me induces a bending of ring A. In the modeling, a BChl *c* aggregate is more open than a BChl *d* aggregate containing 20-H instead of 20-Me.[11,12] Hence, the bulkiness of the side chains might counteract and fine-tune the dense stacking provoked by the coordination and H-bonding. The stereochemistry of the molecule appears to be another crucial factor for the local self-organization in the natural system. Molecular modeling predicts that BChl *c* can form stacks with different conformations, with the Mg ion at the opposite side (anti) or the same side (syn) of the ring plane compared to the 17^1-C.[11] In two layers of BChl *c* with opposite curvatures, an outer anti layer will have ester chains pointing to the exterior, whereas a syn inner layer will have the tails filling the center of a tube.[11,13] The [3^1R] and [3^1S] stereoisomers are thought to stabilize this tubular bilayer structure, where the outer anti layer prefers the [3^1R] and the inner syn layer the [3^1S] form. This represents another tuning mechanism where the chirality of the 3^1-position can play a pivotal role steering the free energy balance of the supramolecular assembly as a whole. Finally, the tails fill the core of the tubular micelles and provide the interface between the tubes.[11,13] They might help to induce the formation of micelles, similarly to fatty acid molecules in an aqueous environment in synergy with the curvatures induced by the 3^1 stereochemistry.

To test for mechanisms controlling the self-organization of BChl *c* in the chlorosomes, we have studied self-assembled chlorins **1** and **2** (Figure 1) with MAS NMR spectroscopy. These synthetic chlorins were uniformly enriched with ^{13}C and ^{15}N, with the exception of the tails. In a converging strategy, several functionalities that are potentially involved in determining the size and topology of the suprastructure are absent or modified in parallel in chlorins **1** and **2**. To obtain insight into how the electronic and structural properties of the central metal ion affect the aggregate structure, the Mg^{2+} ion has been replaced by Cd^{2+}. ^{113}Cd, with a natural abundance of 11%, is a good NMR nucleus and has been used in the past to determine coordination properties in porphyrin compounds,[14−16] heme proteins,[17,18] and photosynthetic membrane protein complexes.[19] The ionization potentials and electron affinities of the Mg^{2+} and Cd^{2+} are different. The ionic radius of Cd^{2+} in a four-coordinated environment is 0.78 Å. This is considerably larger than the 0.57 Å radius of Mg^{2+}. Second, to probe the role of the stereochemistry of the 3-substituent, the 3-(1-hydroxyethyl) is replaced by a 3-hydroxymethyl without chirality, while the chirality of the 17- and 18-side chains is unaffected. Third, the 12-side group of the chlorins is a methyl, whereas in the chlorosomes of *Chlorobium tepidum*, an ethyl side chain is present in ca. 98% of the BChl *c*.[7] Fourth, the model molecules have a hydrogen at C-20, instead of the 20-Me, similar to BChl *d*. MAS NMR spectroscopy can be used to determine whether this yields a short plane-to-plane distance. Finally, the long farnesyl chains are truncated by an unlabeled Me in chlorin **1**, which is expected to influence the suprastructure of the aggregate. The chlorin **2** molecule contains a long stearyl tail. If the tails are responsible for the micellar structure in the chlorosomes, this should develop from the structure of self-aggregated chlorin **2**.

It is shown herein that it is possible to resolve the structures of these model systems in great detail using MAS NMR spectroscopy combined with molecular modeling and ring-current shift calculations. The results corroborate the current picture that the stereochemistry of the 3-substituent gives a predominant contribution to the free energy balance that leads to tubular structures in the chlorosomes.

Materials and Methods

^{13}C, ^{15}N-labeled chlorophyll *a* was extracted from *Chlorella vulgaris* K-22 strain cultured in a labeled medium (Chlorella Industry Co. Ltd.) and converted to methyl ^{13}C, ^{15}N-labeled pyropheophorbide *a* by use of unlabeled methanol.[20] Using the resulting methyl ester as the starting material, cadmium methyl ^{13}C, ^{15}N-labeled 3^1-demethyl bacteriopheophorbide *d* (chlorin **1**) was prepared.[21] According to related procedures,[22] the methyl ester was exchanged with the unlabeled stearyl ester to produce stearyl ^{13}C, ^{15}N-labeled pyropheophorbide *a*, followed by transformation of the 3-vinyl to a 3-hydroxymethyl group. The resulting compound was metalated similarly to the preparation of chlorin **1** to give the corresponding cadmium complex (chlorin **2**). Samples for MAS NMR measurements were prepared by adding dichloromethane/methanol (3:1) until the solids were completely dissolved. Hexane was added in excess (10:1) to the monomer solutions. The aggregates precipitated immediately. The aggregates were filtered, washed with chloroform, and dried in vacuo for several hours. All procedures were performed at room temperature (ca. 20.0 °C).

Solid-state MAS NMR experiments were performed at a temperature of 277 K with DMX-400 and DSX-750 spectrometers, using 4-mm triple resonance MAS probeheads (Bruker, Karlsruhe, Germany). The spinning frequency was kept constant within a few hertz. Ramped variable-amplitude cross-polarization (VACP)[23] with a recycle delay of 1 s was applied in all experiments. The ^{1}H spins were decoupled during acquisition using two-pulse phase modulation (TPPM).[24] Homonuclear ^{13}C−^{13}C dipolar correlation spectra were recorded using radio-frequency-driven dipolar recoupling (RFDR) with phase-sensitive detection in ω_1.[25] ^{1}H 90° pulses of 3.5 μs were used with cross-polarization (CP) periods of 2 ms. For each of 256 steps in the indirect dimension, eight transients were accumulated. Heteronuclear ^{1}H−^{13}C correlations were obtained by wide-line separation (WISE) and phase-modulated Lee−Goldburg (PMLG) experiments using short CP times of 128 or 256 μs and an ^{1}H 90° pulse of 3.1 μs. The ^{1}H chemical shift scale was calibrated from a PMLG spectrum of solid tyrosine·HCl salt. For each of 128 steps in the indirect ^{1}H dimension, four ^{13}C transients were accumulated, while during the WISE experiment, 64 ^{13}C transients were accumulated for each of 32 ^{1}H steps. A 3D ^{1}H−^{13}C−^{13}C WISE/RFDR experiment was performed using an ^{1}H rf field of 81 kHz, a ^{13}C rf field of 45 kHz, and a VACP interval of 128 μs. For each of 16 steps in the indirect ^{1}H dimension and for 256 steps in the indirect ^{13}C dimension, 16 ^{13}C transients were accumulated. 1D ^{15}N CP/MAS experiments were performed with variable-amplitude CP periods of 5.12 ms. For each experiment, 1024 transients were accumulated. Solid-state ^{113}Cd

shifts were referenced to 0.1 M $Cd(ClO_4)_2$ in H_2O by setting the ^{113}Cd response of solid $Cd(ClO_4)_2 \cdot 6H_2O$ to −9 ppm.[26] ^{113}Cd CP/MAS experiments employed VACP times of 2 ms for the acquisition of ∼15000 scans. ^{113}Cd and ^{15}N chemical shielding tensor elements were determined from the spinning sideband pattern of 1D CP/MAS spectra following the Herzfeld and Berger procedure.[27] Error margins were estimated by repeating the experiment with different spinning frequencies and by an interactive tensor analysis.[28] CHHC experiments were performed using an ^1H rf field of 71 kHz and VACP periods of 64 μs.[29] For 256 indirect ^{13}C steps, 16 transients were acquired. A 3D WISE/CHHC experiment used an ^1H rf field of 81 kHz and three VACP periods of 96 μs. One hundred twenty-eight scans were acquired for each of 144 indirect ^{13}C steps and 12 ^1H steps.

To determine the shifts of the monomer in solution, NMR experiments were performed in coordinating solvents with concentrations of ca. 0.01 M.[30] The NMR data for the monomer in dimethyl sulfoxide-d_6 (DMSO) and in tetrahydrofuran-d_8 (THF) were acquired with a DMX-600 spectrometer (Bruker, Karlsruhe, Germany). The ^{15}N chemical shifts were referenced to liquid NH_3. The chemical shifts were used to calculate the aggregation shifts $\Delta\sigma = \sigma_i - \sigma_{liq}$ for ^1H and ^{13}C. The ^{15}N and ^{113}Cd responses were measured in DMSO. The ^{113}Cd chemical shifts were referenced to 0.1 M $Cd(ClO_4)_2$ in H_2O. A single ^{113}Cd signal in DMSO was observed in a 1D experiment, using ∼4000 scans with a recycle delay of 8 s.

Structural modeling was done using the Hyperchem version 7 software (Hypercube, Inc.). All geometry optimizations used a Polak−Ribiere conjugate gradient algorithm with a gradient convergence criterion of 0.01 kcal/mol. DFT calculations of chemical shifts were done using the Gaussian 98 (Gaussian, Inc.) software. For these calculations, a Mg center was used, as Cd is represented poorly compared to Mg in the DFT method, and the H_2O was removed.

To calculate the ring-current effects for intermolecular distances, the macrocycles were approximated by circular loops with a 3-Å radius. The magnetic field $\vec{B}$ induced at a position $\vec{r}$ by a circular loop with current I is given by

$$\vec{B} = \frac{\mu_0 I}{4\pi}\int \frac{\mathrm{d}\vec{l} \times \vec{r}}{r^3} \qquad (1)$$

integrated around the loop in the direction of the current. For a loop with radius a in the xy plane and centered at the origin, the isotropic ring-current shift σ_{rc} is proportional to B_z, yielding

$$\sigma_{rc}(x,y,z) = c\int_0^{2\pi} \mathrm{d}\varphi\left(1 - \frac{x}{a}\cos\varphi - \frac{y}{a}\sin\varphi\right) \times \left[\left(\frac{x}{a} - \cos\varphi\right)^2 + \left(\frac{y}{a} - \sin\varphi\right)^2 + \left(\frac{z}{a}\right)^2\right]^{-3/2} \qquad (2)$$

The ring current of a single loop was calibrated by a nucleus-independent chemical shift (NICS) DFT calculation for a ghost atom placed 4.0 Å above the center of a chlorin molecule, using a B3LYP/6−311G(d,p) level of theory. For these conditions, a ring-current shift of 3.90 ppm was obtained. Using eq 2, this provides c = 2.87 ppm as a calibration constant. The total intermolecular ring-current shift for each ^1H atom was obtained by adding the contribution from all other rings in the lattice within a maximum range r_{max} = 24 Å

$$\sigma_{1H}(x_{1H},y_{1H},z_{1H}) = \sum_{i\neq 0}^{r<r_{max}} \sigma_{rc}(x_{1H} - x_i, y_{1H} - y_i, z_{1H} - z_i) \qquad (3)$$

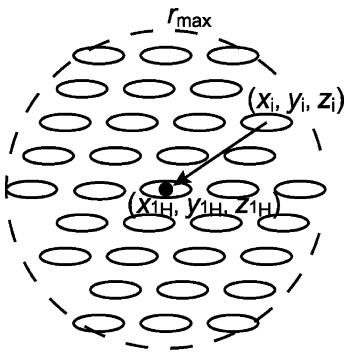

Figure 2. Schematic representation of the lattice summation for the ^1H ring-current shift calculation.

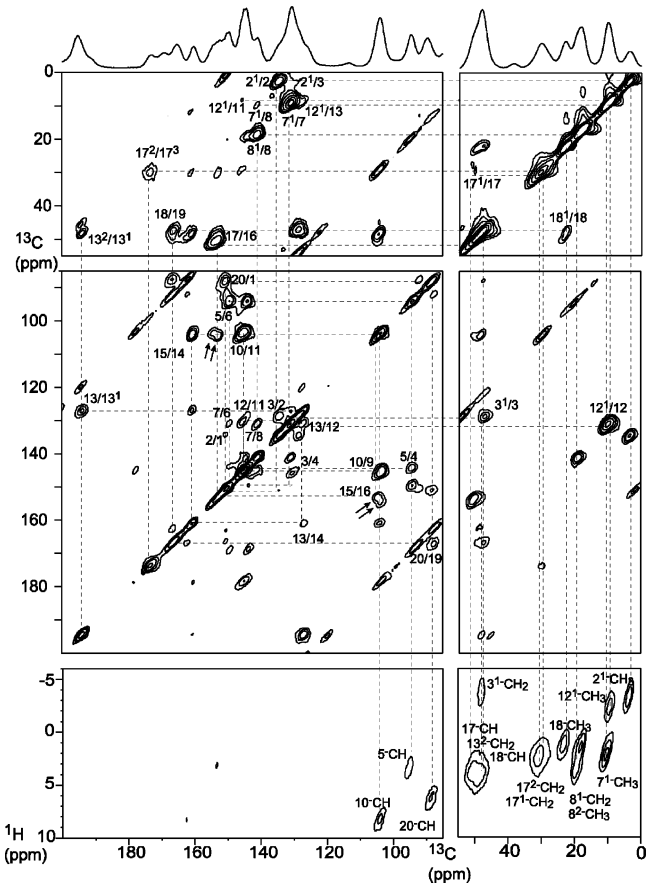

Figure 3. Contour plot sections of a $^{13}C-^{13}C$ MAS NMR dipolar correlation spectrum of aggregated chlorin **2** recorded in a field of 17.6 T using a spinning frequency of 14 kHz and a mixing time of 1.14 ms. The lower panels show contour plot sections of an $^1H-^{13}C$ MAS NMR PMLG dipolar correlation spectrum recorded in the same field employing a spinning rate of 11 kHz. The upper trace shows parts of a 1D CP/MAS spectrum using 12345 Hz MAS. The $^{13}C-^{13}C$ and $^1H-^{13}C$ connectivity network is indicated with dashed lines. The arrows indicate a doubling of the 15/16-C correlation.

where each σ_{rc} given by the integral in eq 2 was evaluated numerically using Maple 6 (Waterloo Maple, Inc.). This summation over a two-dimensional lattice is depicted schematically in Figure 2.

Results

Assignment of the NMR Responses. The chemical shifts of the aggregated chlorins were obtained using 2D and 3D MAS correlation spectroscopy. Figure 3 shows a 2D $^{13}C-^{13}C$ RFDR spectrum of aggregated chlorin **2** recorded with a mixing time

TABLE 1: ^{13}C Chemical Shifts of Chlorins 1 and 2

position	$\sigma_{1,\mathrm{THF}}$	$\sigma_{1,\mathrm{DMSO}}$	$\sigma_{1,i}$	$\sigma_{2,\mathrm{DMSO}}$	$\sigma_{2,i}$
12^1	12.5	12.2	9.2	12.2	9.4
2^1	11.4	10.9	3.3	10.8	3.2
7^1	11.3	10.7	9.8	10.7	10.3
8^2	18.1	17.6	[18.7]	17.5	[19.1]
8^1	20.3	18.7	18.7	18.8	19.7
18^1	23.8	23.0	23.1	23.1	22.6
17^1	31.3	29.6	31.0	29.7	30.6
17^2	31.3	30.2	29.6	30.5	30.1
13^2	49.7	48.3	48.7	48.3	48.6
18	50.6	48.5	47.0	48.5	47.7
17	53.0	50.7	51.2	50.8	50.3
3^1	56.9	54.5	49.0	54.6	47.4
20	92.3	91.7	89.6	91.8	88.3
5	100.3	98.8	94.4	98.9	94.3
15	107.2	105.5	105.0	105.6	103.7, 104.4
10	107.6	106.8	104.1	106.8	104.0
13	131.8	131.0	127.2	131.1	127.0
12	134.2	132.5	131.5	132.5	130.8
7	134.3	133.1	131.1	133.0	130.8
2	136.9	136.3	135.3	136.2	134.2
3	142.6	141.5	130.3	141.4	128.7
8	144.4	143.6	142.6	143.5	140.9
9	147.2	145.6	144.6	145.5	144.7
11	149.3	147.2	145.3	147.2	145.8
4	149.4	148.4	144.6	148.4	144.5
6	152.8	151.5	150.0	151.6	149.6
1	155.4	154.0	151.4	154.0	150.8
16	156.7	155.9	152.5	155.9	152.8, 154.1
14	162.8	161.1	161.6	161.0	160.9
19	169.2	168.8	166.7	168.7	166.7
17^3	173.8	173.2	175.2	172.8	173.7
13^1	195.1	195.2	195.5	195.1	194.4

of 1.14 ms. A spectrum of aggregated chlorin **1** recorded under similar experimental conditions shows almost identical results (data not shown). The nearest-neighbor connectivities of the molecular ^{13}C network lead to the assignment indicated with the dashed lines in Figure 3. The spectrum of chlorin **1** has a single set of narrow peaks with line widths of 220−300 Hz in a field of 9.4 T, and the line widths are only ∼10% higher in a field of 17.6 T. This provides evidence for a well-defined microcrystalline structure without major inhomogeneous broadening due to disorder. The ^{13}C line widths of aggregated chlorin **2**, however, of 200−300 Hz in a field of 9.4 T are increased by ∼50% in a field of 17.6 T, which indicates a significantly increased inhomogeneous broadening and disorder in the sample. In addition, a doubling of the 15/16 correlation is resolved (Figure 3).

Relayed transfer from the 2^1-, 7^1-, and 12^1-carbons to their second-nearest neighbors allowed the unambiguous assignment of those methyl signals. The 2^1/3, 7^1/8, 12^1/11 and 12^1/13 correlations are weakly visible in Figure 3. The 8^1 response could not be resolved from the 8^2-^{13}C signal. The 4-, 6-, 9-, and 11-positions were assigned from relayed transfer correlations using a dataset recorded with a relatively long mixing time of 2.9 ms. The 11-carbon can be assigned from a relayed 12^1/11 correlation in Figure 3. The ^{13}C chemical shifts of the aggregated chlorins are summarized in Table 1.

For the assignment of the ^{1}H shifts, the PMLG[31] technique was applied in a high field of 17.6 T. Using the ^{13}C data as a starting point, the ^{1}H−^{13}C signals were assigned, as depicted in the lower panels of Figure 3 for chlorin **2**. The 3^1-OH proton is not observed, possibly because of some form of dynamics resulting in excessive line broadening and inefficient CP. Several signals are difficult to assign because of overlap in the ^{13}C dimension. In particular, there is overlap between 7^1-CH_3 and 12^1-CH_3 and between the 3^1-CH_2 and 13^2-CH_2 in the ^{13}C

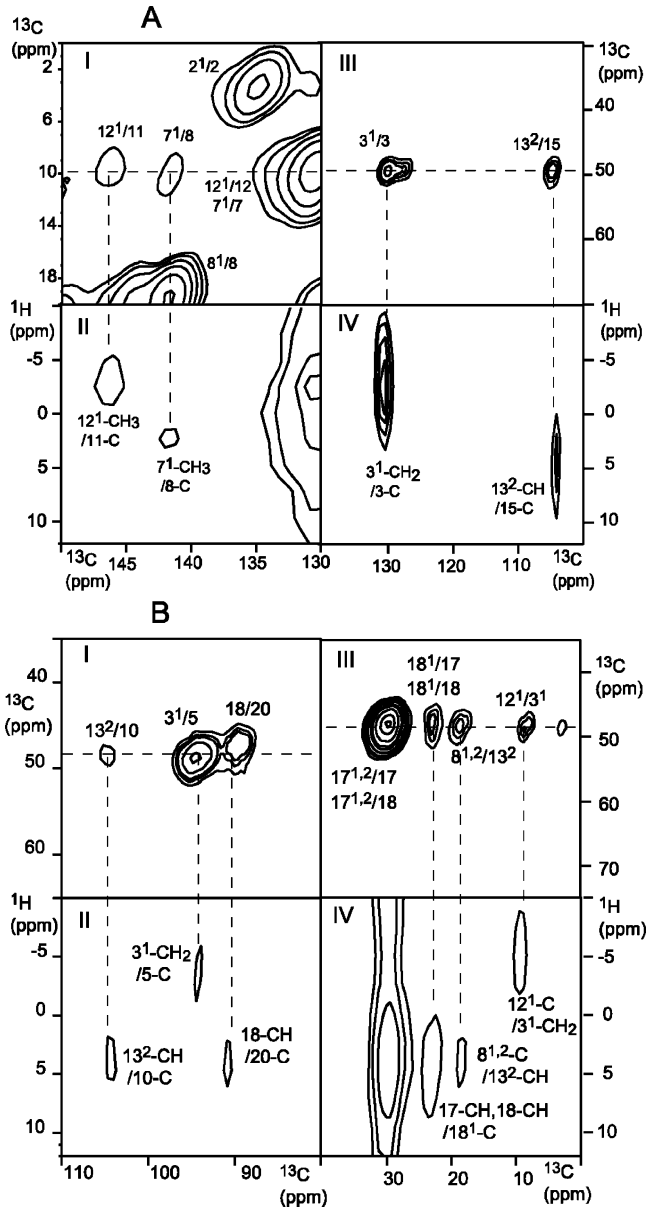

Figure 4. (A) Enlarged ^{13}C−^{13}C sections of a 2D RFDR spectrum of aggregated chlorin **1** recorded in a field of 9.4 T employing a spinning frequency of 11 kHz (I, III) and ^{1}H−^{13}C slices of a 3D ^{1}H−^{13}C−^{13}C WISE/RFDR spectrum recorded in a field of 17.6 T employing a spinning frequency of 14 kHz (II, IV). In spectrum II (IV), the ^{13}C shift in the third dimension is 9.5 (49) ppm, as indicated by the horizontal dashed line in spectrum I (III). (B) Enlarged ^{13}C−^{13}C sections of Figure 7A (I, III), and ^{1}H−^{13}C slices of a 3D ^{1}H−^{13}C−^{13}C WISE/CHHC spectrum of aggregated chlorin **1** recorded in a field of 17.6 T using a spinning frequency of 14.5 kHz (II, IV), where the chemical shift of the indirect ^{13}C dimension is 49 ppm, as indicated by the horizontal dashed lines in spectra I and III.

dimension. To complete the solid-state ^{1}H assignment, a 3D ^{1}H−^{13}C−^{13}C dataset was collected for chlorin **1**. A straightforward WISE step was implemented after the initial ^{1}H 90° pulse in the sequence.[11] With a short CP time of 128 μs, cross-peaks appear in the 3D spectrum that correlate an ^{1}H spin to a directly bound ^{13}C pair. In the ^{1}H WISE dimension, most peaks are already well resolved because of the truncation of the ^{1}H dipolar couplings in the high field. In Figure 4A, two sections of a 2D ^{13}C−^{13}C spectrum are shown (panels I, III) together with the corresponding ^{1}H−^{13}C slices from the 3D experiment (panels II, IV). The horizontal dashed lines in panels I and III in Figure 4A correspond to the ^{13}C shifts of the ^{1}H−^{13}C slices

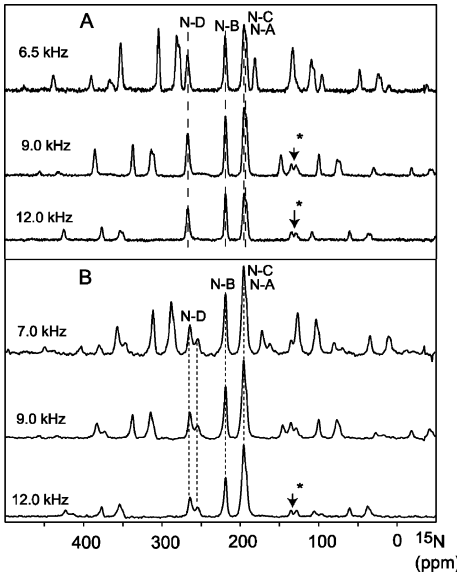

Figure 5. 1D ^{15}N CP/MAS spectra of aggregated (A) chlorin **1** and (B) chlorin **2** recorded in a field of 17.6 T employing different spinning frequencies. The isotropic contributions are connected by dashed lines. The asterisks denote small fractions of the samples where the macrocycles do not contain Cd.

TABLE 2: ^{1}H Chemical Shifts of Chlorins 1 and 2 and Calculated Ring-Current Shifts (ppm)

position	$\sigma_{\mathbf{1},\mathrm{THF}}$	$\sigma_{\mathbf{1},\mathrm{DMSO}}$	$\sigma_{\mathbf{1},i}$	$\sigma_{\mathbf{2},\mathrm{DMSO}}$	$\sigma_{\mathbf{2},i}$	σ_{calc}
12^1-H_3	3.6	3.5	−1.7	3.5	−2.3	−4.8
2^1-H_3	3.3	3.2	−2.8	3.2	−3.3	−5.6
7^1-H_3	3.2	3.2	3.0	3.2	2.1	−0.1
8^2-H_3	1.7	1.6	3.3	1.6	1.5	0.1
8^1-H_2	3.8	3.7	3.3	3.7	3.4	−0.1
18^1-H_3	1.7	1.7	2.1	1.7	4.1	−0.3
17^1-H_2	2.4	2.7	2.7	2.7	2.4	−1.4
17^2-H_2	2.4	2.5	2.7	2.5	2.4	0.0
13^2-H_2	4.9, 5.2	4.9, 5.2	4.2	4.9, 5.2	3.9	−3.2
18-H	4.6	4.5	4.6	4.5	4.1	−0.3
17-H	4.2	4.2	4.2	4.2	3.9	−0.9
3^1-H_2	5.7	5.6	−4.3	5.6	−3.9	−8.1
20-H	8.4	8.4	6.7	8.4	6.2	−1.5
5-H	9.4	9.3	3.8	9.3	3.3	−3.6
10-H	9.5	9.5	8.5	9.5	8.1	−1.6

depicted in panels II and IV. As a result of the first transfer step from ^{1}H to ^{13}C in the 3D experiment, only the bound ^{13}C is correlated with this ^{1}H signal in the ^{1}H−^{13}C−^{13}C dataset. This is illustrated by the labels in panels II and IV. With the 3D datasets, all protons can be assigned unambiguously, while the 2D PMLG spectra provide the most accurate chemical shifts. The ^{1}H chemical shifts of the aggregated chlorins **1** and **2** are summarized in Table 2.

To obtain the ^{1}H and ^{13}C aggregation shifts, defined as the chemical shifts in the solid state relative to the monomer shifts in solution, chlorin **1** was dissolved in THF-d_8 and DMSO-d_6, which are strong coordinating solvents, and chlorin **2** was dissolved only in DMSO-d_6. The ^{1}H and ^{13}C assignments were obtained from 1D ^{1}H and ^{13}C experiments, as well as 2D ^{1}H−^{13}C and ^{13}C−^{13}C COSY experiments. The ^{13}C and ^{1}H monomer shifts are listed in Tables 1 and 2, respectively.

Figure 5 shows ^{15}N CP/MAS spectra of the aggregates. To assign the ^{15}N response, long-range ^{1}H−^{15}N heteronuclear multibond correlation (HMBC) experiments were done for the monomeric species dissolved in DMSO-d_6, where the ^{15}N spins are correlated with the ^{1}H spins at the 5-, 10- and 20-meso-positions. The assignment of the ^{15}N signals in Figure 5 is based on the response in solution (Table 3). The distinction between

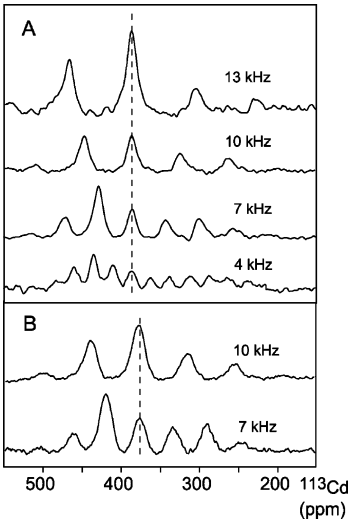

Figure 6. ^{113}Cd CP/MAS spectra of aggregated (A) chlorin **1** and (B) chlorin **2** recorded in a field of 17.6 T employing different spinning frequencies. The isotropic contributions are connected by a dashed line.

TABLE 3: ^{15}N Chemical Shifts and Tensor Elements (ppm) with the Associated Anisotropy and Asymmetry Parameters of Chlorins 1 and 2

position	σ_{DMSO}	σ_i	σ_{11}	σ_{22}	σ_{33}	δ (kHz)	η
(**1**) N-A	192.7	193.0[a]	324	278	−22	−25	0.21
(**1**) N-B	221.6	219.3	421	265	−28	−28	0.63
(**1**) N-C	197.6	195.5[a]	347	265	−24	−25	0.37
(**1**) N-D	264.2	267.2	500	304	−3	−31	0.73
(**2**) N-A	193.3	192.8[b]	353	251	−18	−24	0.48
(**2**) N-B	222.2	218.8	406	266	−16	−27	0.60
(**2**) N-C	198.2	195.5[b]	353	251	−18	−24	0.46
(**2**) N-D	265.0	254.3, 264.3	472, 496	280, 290	10, 8	−28, −29	0.79, 0.80

[a] N-A and N-C could be interchanged. [b] N-A and N-C not fully resolved.

the N-A and N-C is ambiguous, given that the chemical shift difference in solution is small. The ^{15}N chemical shifts and estimated tensor elements are summarized in Table 3. The ^{15}N spectra of aggregated chlorin **1** show a single set of peaks. In the ^{15}N MAS NMR spectra of chlorin **2**, however, a doubling of the N-D peak is observed.

In the ^{113}Cd CP/MAS spectra, a broad signal appears at 395 ppm for chlorin **1**, compared to 375 ppm for chlorin **2** (Figure 6). The chemical shift tensor elements and anisotropy and asymmetry parameters that were estimated from the spinning sidebands in Figure 6 are listed in Table 4. Finally, the ^{113}Cd response in DMSO-d_6 for chlorin **1** shows a single peak at 390 ppm (Table 4).

Recently, it has been shown that good long-range ^{13}C−^{13}C transfer can be obtained using an ^{1}H spin diffusion interval sandwiched between two additional CP steps.[32,33] Figure 7 shows 2D spectra of aggregated chlorin **1** (A) and chlorin **2** (B) recorded with a CHHC experiment that was adapted for short mixing times.[29,34] An ^{1}H spin diffusion interval of 0.2 ms was used to generate ^{13}C−^{13}C correlations. The assignment of the correlations in Figure 7 is straightforward with the ^{13}C shifts of Table 1, with the exception of ambiguities due to overlap between the 3^1- and 13^2-carbons and between the 7^1- and 12^1-carbons. To resolve these ambiguities, a 3D WISE/CHHC experiment was implemented by including an additional ^{1}H evolution period after the initial ^{1}H 90° pulse. Figure 4B shows two sections from the 2D CHHC experiment (panels I, III), together with the corresponding ^{1}H−^{13}C slices of the 3D

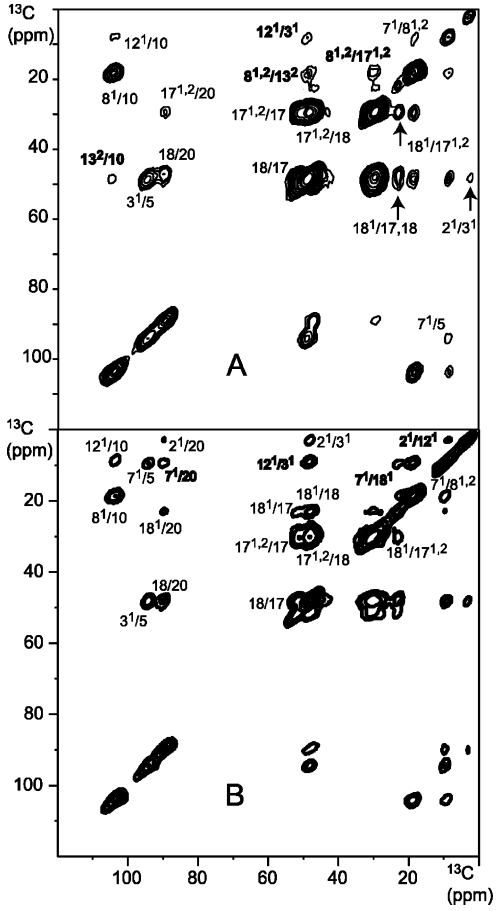

Figure 7. $^{13}C-^{13}C$ CHHC spectra of aggregated (A) chlorin **1** and (B) chlorin **2** recorded in a field of 9.4 T using a spinning frequency of 11 kHz and an ^{1}H spin diffusion mixing time of 200 μs. The correlations labeled in bold face are assigned as intermolecular.

spectrum (panels II, IV) of chlorin **1**. With the additional information contained in the 3D dataset, the cross-peaks are assigned as indicated in Figure 7A. The weak signals assigned to $7^1/8^{1,2}$ and $7^1/5$ correlations are not detected in the 3D experiment, and the assignment is tentative. Using the ^{13}C shifts from Table 1 and the information in Figure 7A, all signals are assigned correspondingly in Figure 7B for aggregated chlorin **2**.

Aggregation Shifts. Significant upfield ^{1}H and ^{13}C aggregation shifts are observed and displayed as circles for values less than -2.5 ppm in Figure 8 relative to the monomer in DMSO. For chlorin **1**, two sets of ^{13}C monomer shifts were determined both in DMSO and in THF. The ^{13}C shifts show significant differences when comparing the two solvents (Table 1). In contrast, the ^{1}H shifts are very similar for both solvents (Table 2). In addition, Figure 9 compares the ^{1}H and ^{13}C chemical shifts for the aggregated chlorin **1** with the shifts for the monomer in DMSO. These correlation plots clearly show how pronounced the ^{1}H aggregation shifts are within the ^{1}H chemical shift range, in contrast to the ^{13}C aggregation shifts. The ^{1}H aggregation shifts are dominated by ring-current effects, in line with observations in other chlorophyll aggregates, and are more useful than the ^{13}C shifts for structure determination.[30] In particular, the ^{1}H aggregation shifts that are far from the diagonal in Figure 9 are important for structure determination.

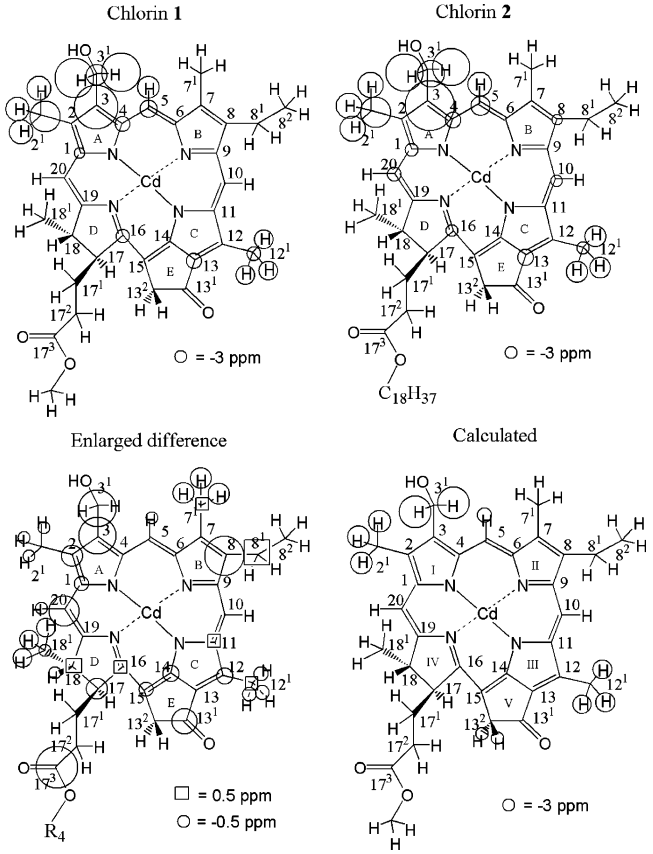

Figure 8. Detected ^{1}H and ^{13}C upfield aggregation shifts of aggregated chlorin **1** and **2** relative to the monomers in DMSO-d_6, the enlarged difference between the two chlorins, and calculated ^{1}H ring-current shifts > 2.5 ppm. The circles have a radius proportional to the magnitude of the shift.

To explain the aggregation shift patterns, structural models of coordinating chlorins were built.[12,35] First, the modeling of sheets of molecules was done along very similar lines for chlorins **1** and **2**. The semiempirical ZINDO/1 method suitable for transition metals[36] was used to calculate the atomic charges for subsequent MM+ force field optimization of the geometries, which was iterated until self-consistent structures were obtained. In this way, trimers were constructed by coordination of 3-hydroxymethyl oxygen to the Cd ion of the neighboring macrocycle, where the remaining third macrocycles were capped by a H_2O as a fifth ligand and optimized in ca. five iteration steps. For larger structures, only the geometry was optimized with MM+. Pentamers were constructed by replacing the central molecules by three of its own copies. The charge of these molecules was negligible, the total charge thus remaining zero. Larger aggregates were built by placing multiple stacks together with the 3^1-OH groups of one stack within hydrogen-bonding distance of the 13-C═O moieties of the next stack, followed by optimization with the MM+ force field. In this way, 26-mers of chlorin **1** and **2** were optimized consisting of four pentamer stacks and two trimer stacks at the outermost positions. Figure 10 shows the central part of the resulting structure of chlorin **1**. The Cd−Cd distance is 6.4 Å, while the O···H distance is approximately 2.2 Å. A Cd−Cd distance of 6.4 Å is well in line with electron diffraction data.[21] Layers of chlorin **2** are arranged similarly (see also Figure 11).

TABLE 4: ^{113}Cd Chemical Shifts (ppm) with the Associated Anisotropy and Asymmetry Parameters

chlorin	σ_{DMSO}	σ_i	σ_{11}	σ_{22}	σ_{33}	δ (kHz)	η
1	390	395 ± 3	494 ± 15	454 ± 15	238 ± 15	-39 ± 5	0.25 ± 0.13
2	nd	375 ± 3	484 ± 15	414 ± 15	228 ± 15	-37 ± 5	0.50 ± 0.16

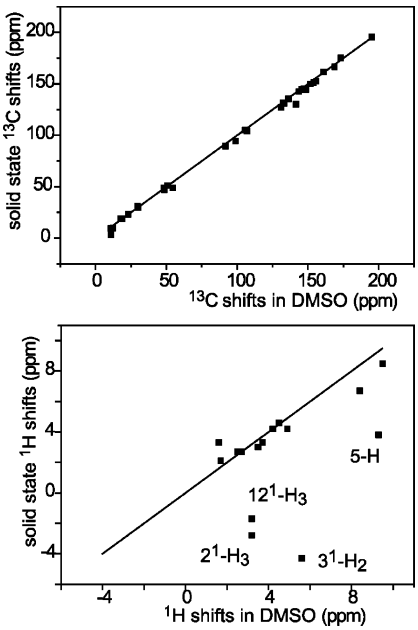

Figure 9. Chemical shift correlation plots of chlorin **1**. The ^{1}H and ^{13}C shifts in the solid sample are plotted against the monomer shifts in a DMSO solution. The solid lines represent the diagonals. Several ^{1}H signals are indicated that show a large upfield shift in the solid relative to the monomer.

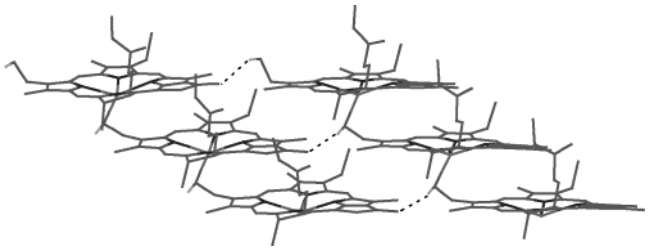

Figure 10. Structure of a layer of parallel inclined stacks of chlorin **1** used for the ring-current shift calculation.

Subsequently, the layer structure of Figure 10 was used for a ring-current shift calculation. A molecule within the center of the 26-mer was selected, and the positions of the neighboring macrocycles were used to define the unit cell of a two-dimensional lattice. The ^{1}H ring-current shifts were calculated with the circular loop model and taking into account contributions within $r_{max} = 24$ Å. The results (Figure 8, Table 2) are in semiquantitative agreement with the NMR measurements and reproduce the essential features, in particular the combination of very strong aggregation shifts in the 3-CH_2 region and significant 12-CH_3 shifts. About 50% of the magnitude of the observed ring-current shifts can be attributed to neighbor molecules within the same stack. Another contribution of ~30% in the 3^{1}- and 12^{1}-regions originates from molecules in adjacent stacks overlapping because of the hydrogen bonding between the parallel inclined stacks (Figure 10). Finally, the ring currents induced over larger distances account for the remaining ~20%. This demonstrates that the cumulative ring-current effects can be very large in aggregated chlorophylls and reveal local microcrystalline order with a correlation length within the plane of a layer of at least ~24 Å.

The aggregation shift patterns for the two chlorins are very similar (Figure 8). The differences in aggregation shifts between the two chlorins, which are depicted enlarged in Figure 8, indicate that the layer structure is marginally perturbed by the presence of the long tails. For example, the shift differences for the 3-, 3^{1}-, and 13^{1}-carbons indicate that the C═O···HO···Cd

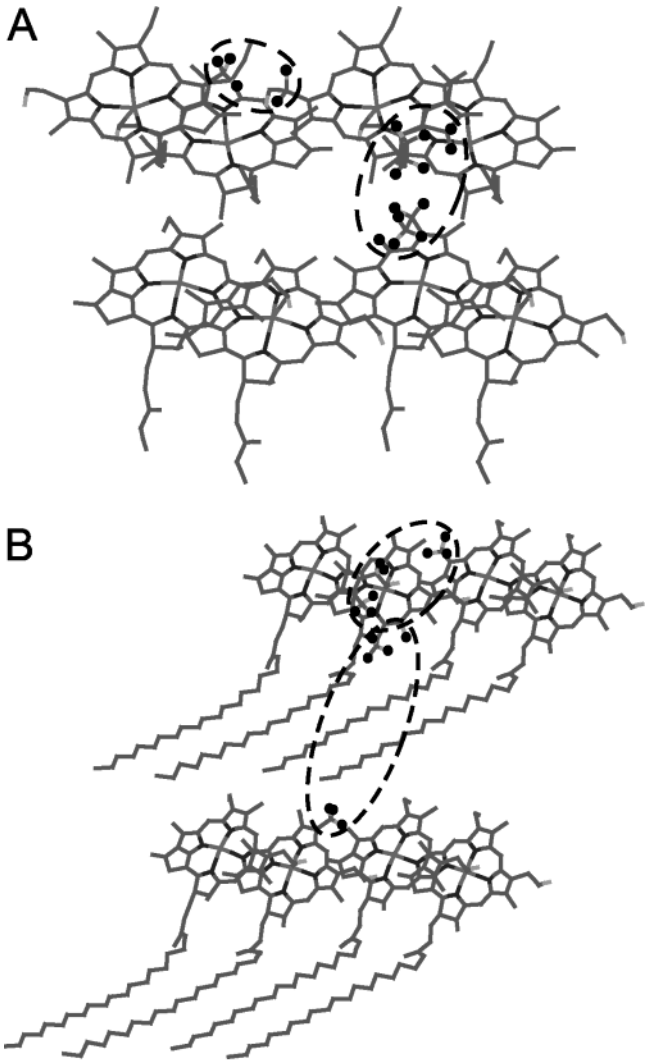

Figure 11. (A) Calculated structure of aggregated chlorin **1** and (B) schematic structure of aggregated chlorin **2** showing two sheets containing two stacks of two molecules each. The black dots represent ^{13}C atoms involved in the intermolecular correlations.

bonding network is affected by the presence of the long stearyl tails. The overall layer structure of Figure 10 is conserved, however, and induces a similar ring-current shift distribution.

Metal Bonding. Previous model studies have shown that the ^{113}Cd CSA tensor is very sensitive to the coordination state of the Cd^{2+} ion. For cadmium *meso*-tetraphenylporphyrin (Cd-TPP), the ^{113}Cd chemical shift anisotropy $\Delta\sigma = \sigma_{||} - \sigma_{\perp}$ is large, $\Delta\sigma = 341$ ppm.[15] The unique tensor element $\sigma_{33} = \sigma_{||}$ is very sensitive to the electronic environment within the plane of the macrocycle. It has a high value of 626 ppm, corresponding to a low electronic shielding. The other two elements, $\sigma_{11} = \sigma_{22} = \sigma_{\perp}$, reflect the axial symmetry of the electronic system. The electronic shielding perpendicular to the porphyrin plane is relatively high, with $\sigma_{\perp} = 285$ ppm. In the pyridine adduct (Py-Cd-TPP), the fifth ligand reduces the anisotropy to $\Delta\sigma = 105$ ppm. In the pyridyl adduct of cadmium protoporphyrin IX dimethyl ester (Cd-PPIXDME-PYR) the coordination is almost axial, with a ^{113}Cd chemical shift asymmetry of $\eta = 0.32$.[17] In Cd-substituted myoglobin, the Cd ion is coordinated by a histidine residue, pulling the Cd strongly out-of-plane. This yields a crossover of $\sigma_{||}$ and $\sigma_{\perp}$ with $\Delta\sigma = -200$ ppm. These findings are supported by ab initio calculations.[18]

The ^{113}Cd signals for the two aggregated chlorins (Figure 6) show a very similar large negative anisotropy (Table 4). In the previous studies, nitrogen was considered as a fifth or sixth ligand, whereas, here, only oxygen is available. However, a similar conclusion as in Cd-substituted myoglobin can be drawn. In particular, $\sigma_{33} = 238$ ppm corresponds to a very high shielding, revealing a weak in-plane Cd−N bonding, with the Cd strongly out-of-plane and five-coordinated. For chlorin **1**, a small value of $\eta = 0.25$ indicates that the axial coordination is somewhat distorted to a degree comparable to that in Cd-PPIXDME-PYR.[17] These findings are in agreement with the layer structure of Figure 10, where the Cd^{2+} ion has the 3^1-OH moiety as a fifth ligand. In addition, the 3^1-OH coordination to the Cd^{2+} ion is not axially symmetric, which explains the observed value of $\eta = 0.25$ for the ^{113}Cd tensor. For chlorin **2**, $\eta = 0.5$ indicates that the Cd^{2+} ion is farther from the central axis.

The ^{15}N isotropic chemical shifts of chlorin **1** in solution as well as in aggregated form (Figure 5, Table 3) are within 10 ppm of the ^{15}N shifts of BChl *c* in methanol, except for the ^{15}N-D signals, which are shifted by up to ∼15 ppm.[37] In pheophytin *a*, where the metal is replaced by H_2, the ^{15}N shifts of the N-A and N-C are decreased by ∼60 ppm compared to Chl *a*, whereas the N-B and N-D ^{15}N shifts are increased by ∼40 ppm.[38] Thus, the ^{15}N data confirm that the metal is bound to the chlorin, although the ^{15}N spectra reveal a small fraction 10% of cadmium chlorin in both samples where the Cd^{2+} ion is replaced by H_2 (Figure 5).[37,38] The ^{15}N shifts show that the Cd−N bonding in aggregated chlorin **1** is very similar to the Mg−N bonding in BChl *c*. The chemical shift tensor elements are also listed in Table 3. Although the anisotropies are approximately similar for the four ^{15}N responses, the asymmetry of N-B and N-D is significantly higher than that for N-A and N-C, which appears to correspond to a stronger Cd−N bonding.

The ^{15}N shifts of chlorin **2** are very similar with the exception of the ^{15}N-D signal, which appears to be doubled in the aggregate with a difference of 10 ppm between the two components, whereas a single component is observed in DMSO (Table 3). For the formation of BChl *c* dimers in CCl_4 solution, it was found that ^{15}N-D is most sensitive and shows a change of 4 ppm.[37] In the chlorosomes, the syn and anti layers are thought to give very similar ring-current shifts, given that they form mirror images with respect to the overlap between the macrocycles.[11] To explore the possibility that the ^{15}N signals are different between the syn and anti configurations, a DFT calculation was performed at the BLYP/6-31G(d,p) level. To estimate the geometries, two monomers of chlorin **1** were optimized by the iterative ZINDO/1 and MM+ method with H_2O as a fifth ligand in either the syn or the anti configuration. The metal−nitrogen distances are quite similar for the two configurations, although the structure of the macrocycle is perturbed. For these approximate syn and the anti geometries, a DFT calculation of the chemical shift was performed.

Table 5 summarizes the calculated ^{15}N shifts for the syn and the anti structures. The ^{15}N-D shift differs by ∼5 ppm between the two structures, while the other three ^{15}N shifts differ by less than 1.5 ppm. Although the absolute calculated ^{15}N shifts agree only moderately with the observed shifts, they clearly show that the ^{15}N-D signal is much more sensitive to the syn or anti configuration than the other ^{15}N signals. In addition, according to the calculation, several ^{13}C signals are also doubled with differences of 1−2 ppm, primarily in the ring-D region (Table 5). Such splittings are difficult to resolve. However, the C-16 resonance in aggregated chlorin **2** is indeed doubled with a difference of 1.3 ppm (Table 1). Thus, the theoretical results are in line with the NMR data and indicate that the aggregated chlorin **2** consists of a mixture of syn and the anti layers.

TABLE 5: Calculated Chemical Shifts (ppm) for the Syn and Anti Isomers, See Text for Details

position	syn	anti
N-A	185.6	184.1
N-B	198.5	199.3
N-C	196.4	196.0
N-D	232.0	227.4
C-10	107.7	106.7
C-16	150.0	151.0
C-17	64.4	62.9
C-18	58.9	60.0
C-20	93.3	94.3
C-17^1	43.8	41.7
C-17^2	44.2	45.6

Intermolecular Contacts. The correlations in Figure 7 are the first to appear for increasing $\tau_m = 0.1-0.2$ ms and are between nearby substituents of chlorin **1** and **2** spanning intramolecular ^{1}H distances d 6 Å. A buildup rate in this range has also been found for a Chl *a*/H_2O aggregate.[39] Many correlations in Figure 7 involve one methyl group in line with the distribution of substituents around the chlorin ring and span short ^{1}H distances of 3 Å. Spin diffusion involving methyls is less efficient because of their fast rotation, which attenuates the dipolar couplings. In contrast, intramolecular correlations between two groups other than methyl are strong and over distances of 6 Å. In particular, the region near the 17-position has several protons forming a network where the spin diffusion proceeds rapidly. Thus, a cross-peak in the CHHC experiments indicates an efficient diffusion pathway between the two spins in a network of protons.

Several correlations in Figure 7 are attributed to intermolecular transfer, because there is no intramolecular pathway in the proton network that can serve to correlate the resonances for $\tau_m = 0.2$ ms. Although the differences between chlorins **1** and **2** are marginal for the intramolecular peaks, more significant differences can be observed for the intermolecular correlations. The $12^1/3^1$ intermolecular correlation in Figure 7A is in excellent agreement with the layer structure in Figure 10, as there are close contacts of ∼2.5 Å between the nearest protons of these side chains (Figure 11). This observation confirms the OH···O═C hydrogen bonding between the stacks. In the chlorin **2** aggregate, additional transfer between the 12^1- and 2^1-carbons is observed, which confirms the perturbation of the C═O···HO···Cd bonding network in the layers. The remaining intermolecular correlations are between the ring-B and ring-D regions located at the opposite sides of a layer. Hence, these correlations involve transfer between adjacent layers in a head-to-tail orientation. The specific correlations between adjacent layers are different between the two aggregates. This is attributed to the presence of the stearyl tails between the layers of chlorin **2**.

In a final step, 3D space-filling structures of the chlorin aggregates can be constructed as a result of these intermolecular correlations. For the microcrystalline chlorin **1** aggregate, multiple layers were brought within van der Waals bonding distance and optimized with the force field. A preliminary communication describing this structure has been published.[40] Figure 11A shows the arrangement of two neighboring layers. The energy of this arrangement was found to be 11 kcal/mol lower for the contact between two molecules in adjacent sheets than for a structure in which the layers are isolated. This indicates favorable van der Waals interactions between the layers. The arrangement in Figure 11A displays a network of

strongly coupled ^{1}H spins in which the 17- and 8-regions are in close contact, in accordance with the observed intermolecular correlations.

According to the NMR data, the aggregated chlorin **2** is more disordered than chlorin **1**. This resembles the chlorosomes, where a significant line broadening is also observed.[11] In the chlorosomes of *Chlorobium tepidum*, however, a splitting pattern around ring-B is observed that is associated with the bilayers.[11] In addition, the observed transfer between the ring-B and ring-D regions in the aggregated chlorins is not consistent with the bilayer structure. In *Chloroflexus aurantiacus*, a monolayered tube with the tails on the exterior side and a central hole was proposed.[41,42] In that case, the cavity should be filled with another low-molecular-weight compound, whereas the in vitro aggregated chlorins form a pure and dry sample. Hence, the experimental evidence strongly favors planar sheets over tubular structures for both cadmium chlorins. The force field method is limited with respect to accurate modeling of the long tails in a large aggregate of chlorin **2**. Figure 11B shows a schematic structure of two adjacent layers of chlorin **2**. The protons of the saturated stearyl chains form a dense three-dimensional network of very strongly coupled ^{1}H spins, which can explain the intermolecular transfer over a relatively large distance. A possible arrangement of bilayers with interdigitating tails, such as in Chl *a*/H_2O,[39,43] was also explored. In the Chl *a*/H_2O aggregate, however, the H_2O molecules form a hydrogen-bonding network within a Chl *a* layer, which makes the layer structure much more open. The chlorin **2** layers are quite dense, making it difficult for the tails to interdigitate. In addition, a doubling of the NMR response of the 7- and 8-substituents is observed in Chl *a* that is associated with conformational changes at the interface between adjacent bilayers, whereas the NMR results of chlorin **2** show single resonances for the 7- and 8-side chains. These results suggest a head-to-tail arrangement of the layers.

Discussion

The organization of layers of BChl *c* in the chlorosomes that is built upon the C═O···HO···Mg network[7,11,12] is conserved in the aggregated cadmium chlorins. This conclusion is also supported by other spectroscopic methods. In particular, the Q_y band is red-shifted, relative to the monomer in a polar solution, by 87 nm for chlorin **1**[21] and by 91 nm for chlorin **2**. This compares well with the shifts of 85 and 88 nm observed for BChl *c* in the chlorosomes and BChl *c* precipitated from hexane, respectively.[1] The stretching frequencies of the 3^1-O−H and the 13-carbonyl C═O at 3140 and around 1640 cm^{-1}, respectively, are from the C═O···HO···Cd network in the aggregated chlorin **1**.[21] Thus, the ligation and H-bond structural motif that is keeping the individual molecules together in the chlorosomal antennae is robust, in the sense that the 5-fold coordination and how it supports the intermolecular bonding network survives the substitution of Mg^{2+} by Cd^{2+}. The density of the layers depends on the bulkiness of the side chains. In particular, the natural BChl *c* has additional 3^1-Me and 20-Me substituents instead of hydrogens and in most cases a 12-Et instead of a 12-Me side group. Because of the less bulky substituents in the cadmium chlorins compared to the Mg forms, the stacking is more dense, which is evident from the exceptionally large aggregation shifts (Figure 8). The plane-to-plane distance is ∼3.5 Å, whereas a distance of ∼4.5 Å was found for BChl *c*.[11] This is corroborated by a recent spectroscopic and molecular modeling study of zinc chlorins in which the effect of various 3^1-substituents was investigated.[35] It was found that the Zn substitute of the Cd analogue has a visible absorption band that is red-shifted to 740 nm compared to 705 nm for the corresponding [3^1*R*] type. Modeling of the latter Zn analogue yielded a plane-to-plane distance of ∼4.1 Å, instead of ∼3.5 Å without the 3^1-Me, which indicates a denser packing if the 3^1-Me is absent.

Although the stacking is essentially similar to the chlorosomal antennae, the differences in molecular structure lead to a different self-organization on the supramolecular scale. The chlorin **1** self-aggregates with a microcrystalline order, and layers of chlorin are arranged in a head-to-tail orientation, in contrast with the tubular structures in the chlorosomes. The NMR data suggest that aggregated chlorin **2** is more disordered and both layers with syn and with anti stacking are found.

These differences of global self-organization reveal the essential factors controlling the tubular organization in the chlorosomes. First, in the chlorosomes, the 3^1-Me introduces the [3^1*R*] and [3^1*S*] stereoisomers. For various bacteriochlorophylls, it has been found that the formation of higher aggregates and the degree of structural similarity to the chlorosomes depends on the 3^1-epimeric composition of the solution.[44−56] In the chlorosomes of *C. tepidum*, the 3^1 stereoisomers interact with the syn and anti configuration of the metal ion in the sense that a [3^1*S*]-syn inner layer surrounded by a [3^1*R*]-anti outer layer is thought to stabilize the tubular micelles.[11] In addition, in a study of the aggregation of BChl *e*, it was found that a minimal amount of the [3^1*S*] stereoisomer is required for the formation of aggregates resembling the chlorosomal antennae.[13,48] In particular, upon addition of the [3^1*S*] stereoisomer to a [3^1*R*] BChl *e* aggregate, the Q_y absorption band shifts from 706 to 717 nm, indicating the reorganization from a lower aggregate to a chlorosome-like aggregate. The subtle interplay between the [3^1*R*] and [3^1*S*] stereoisomers that appears to be essential for the formation of the tubular micelles is absent in the cadmium chlorins. Without the 3^1-Me, the cadmium chlorin molecules have mirror symmetry with respect to the ring plane, with the exception of the ring-D substituents, which are less important for the intermolecular binding. This points to the critical role for the 3-side chain, and the changes in the suprastructure are primarily attributed to the substitution of the 3-(1-hydroxyethyl) moiety with a 3-hydroxymethyl group lacking the 3^1-chirality.

The tails constitute another factor that is of interest to the suprastructure. In chlorin **1**, the tails are truncated by a methyl. The structural modeling results suggest favorable weak interactions between the layers oriented head-to-tail, where the truncated tails perfectly fill the space between the 8-Et and 7-Me groups of the neighboring layer. In this way, a microcrystalline solid can be formed. In the aggregated chlorin **2**, the suprastructure is different as a result of the tails. Although the stearyl tail does not have any significant interaction with the other substituents in a single molecule, it contributes to the entropic and interfacial energy terms in the free energy balance. The tails alone are apparently not sufficient for tubular micelles. In this respect, the chlorosomal antennae are different from micelles of fatty acids. On the other hand, the tails induce structural disorder in the aggregate. As a result of this disorder, layers with both syn and anti stacking are formed, which resembles the chlorosomes.

Conclusions

Synthetic cadmium chlorins **1** and **2** were self-aggregated in cyclohexane and studied to gain insight into how key functionalities can steer the suprastructure of BChl *c* aggregation in the

chlorosomes. With various MAS NMR experiments in combination with molecular modeling and ring-current shift calculations, local structures were found that are similar to the stacking of BChl *c* in the chlorosomes at the molecular level, although the supramolecular structure of tubular micelles is not formed. The aggregate chlorin **1** with the truncated tails appears to be microcrystalline with a monoclinic local symmetry. The aggregate chlorin **2** with the long stearyl tails is more disordered, and the NMR response suggests the presence of both syn and anti layers. With these structures, several key factors controlling the self-organization in the chlorosomes can be designated. The Cd···OH···O═C motif induces self-organization in a robust bottom-up process in essentially the same fashion as the Mg···OH···O═C moieties in the chlorosomes. The packing of the molecules in sheets is more dense than for the chlorosomes and gives rise to very strong ring-current shifts. The high density is attributed mainly to the 3^1- and 20-substituents, which are less bulky than in the chlorosomes. A quantitative analysis of the ring currents, including non-nearest-neighbor effects, validates the layer structure that was built by molecular modeling. Intermolecular $^{13}C-^{13}C$ correlations provide a conclusive validation of the space-filling model structures. Sheets of chlorin are oriented head-to-tail in the aggregates. The model structures identify the 3-moiety in BChl *c* as a prerequisite for tubular suprastructure. It is envisaged that the [3^1R] and [3^1S] stereoisomers in the chlorosomes break the symmetry of the planar sheets and give rise to terms in the free energy balance that favor a tubular structure. The truncated tails in chlorin **1** lead to a microcrystalline structure. In contrast, the stearyl tails of chlorin **2** induce structural effects that resemble the chlorosomal antennae, in particular the presence of syn and anti layers. This suggests that the long tails are also needed for the formation of the antennae, probably because of the many weak interactions between the hydrogens of adjacent chains or the contribution of the flexible chains to the entropy of the system. In conclusion, this study shows how a balance of strong local interactions in a bottom-up process and terms in the free energy balance associated with a longer distance scale is responsible for this supramolecular assembly, which provides a view on evolutionary selection and might be of interest to future design of artificial structures.

Acknowledgment. The authors thank F. Lefeber and J. Hollander for assistance during the experimental work. M. Amakawa is acknowledged for his contribution to the synthesis. Alia, J. Pauli, G. Nachtegaal, and A. P. M. Kentgens are acknowledged for their contributions during the early stages of the project. M. Umetsu is thanked for stimulating discussions. J.M. acknowledges a Casimir−Ziegler award of the Academies of Sciences in Amsterdam and Düsseldorf. H.J.M.d.G. is a recipient of a PIONIER award of the chemical sciences division of The Netherlands Organization for Scientific Research (NWO). The 750-MHz wide-bore instrumentation was financed in part by Demonstration Project BIO4-CT97-2101 of the Commission of the European Community. This work was partially supported by Grants-in-Aid for Scientific Research (No. 15033271) on Priority Areas (417) from the Ministry of Education, Culture, Sports, Science and Technology (MEXT) of the Japanese Government and for Scientific Research (B) (No. 15350107) from the Japanese Society for the Promotion of Science (JSPS).

References and Notes

(1) Olson, J. M. *Photochem. Photobiol.* **1998**, *67*, 61−75.
(2) Müller, M. G.; Griebenow, K.; Holzwarth, A. R. *Biochim. Biophys. Acta* **1993**, *1144*, 161−169.
(3) Mimuro, M.; Nishimura, Y.; Yamazaki, I.; Kobayashi, M.; Wang, Z. Y.; Nozawa, T.; Shimada, K.; Matsuura, K. *Photosynth. Res.* **1996**, *48*, 263−270.
(4) van Grondelle, R.; Decker, J. P.; Gillbro, T.; Sundstrom, V. *Biochim. Biophys. Acta* **1994**, *1187*, 1−65.
(5) Griebenow, K.; Holzwarth, A. R.; van Mourik, F.; van Grondelle, R. *Biochim. Biophys. Acta* **1991**, *1058*, 194−202.
(6) Staehelin, L. A.; Golecki, J. R.; Drews, G. *Biochim. Biophys. Acta* **1980**, *589*, 30−45.
(7) Balaban, T. S.; Holzwarth, A. R.; Schaffner, K.; Boender, G. J.; de Groot, H. J. M. *Biochemistry* **1995**, *34*, 15259−15266.
(8) Blankenship, R. E.; Olson, J. M.; Miller, B. *Anoxygenic Photosynthetic Bacteria*; Kluwer Academic Publishers: Dordrecht, The Netherlands, 1995.
(9) Hildebrandt, P.; Tamiaki, H.; Holzwarth, A. R.; Schaffner, K. *J. Phys. Chem.* **1994**, *98*, 2192−2197.
(10) Brune, D. C.; Nozawa, T.; Blankenship, R. E. *Biochemistry* **1987**, *26*, 8644−8652.
(11) van Rossum, B. J.; Steensgaard, D. B.; Mulder, F. M.; Boender, G. J.; Schaffner, K.; Holzwarth, A. R.; de Groot, H. J. M. *Biochemistry* **2001**, *40*, 1587−1595.
(12) Holzwarth, A. R.; Schaffner, K. *Photosynth. Res.* **1994**, *41*, 225−233.
(13) Steensgaard, D. B.; Wackerbarth, H.; Hildebrandt, P.; Holzwarth, A. R. *J. Phys. Chem. B* **2000**, *104*, 10379−10386.
(14) Ellis, P. D.; Inners, R. R.; Jakobsen, H. J. *J. Phys. Chem.* **1982**, *86*, 1506−1508.
(15) Jakobsen, H. J.; Ellis, P. D.; Inners, R. R.; Jensen, C. F. *J. Am. Chem. Soc.* **1982**, *104*, 7442−7452.
(16) Rodesiler, P. F.; Griffith, E. A. H.; Charles, N. G.; Lebioda, L.; Amma, E. L. *Inorg. Chem.* **1985**, *24*, 4595.
(17) Kennedy, M. A.; Ellis, P. D. *J. Am. Chem. Soc.* **1989**, *111*, 3195−3203.
(18) McAteer, K.; Lipton, A. S.; Kennedy, M. A.; Ellis, P. D. *Solid State Nucl. Magn. Reson.* **1996**, *7*, 229−238.
(19) Matysik, J.; Alia; Nachtegaal, G.; van Gorkom, H. J.; Hoff, A. J.; de Groot, H. J. M. *Biochemistry* **2000**, *39*, 6751−6755.
(20) Tamiaki, H.; Amakawa, M.; Shimono, Y.; Tanikaga, R.; Holzwarth, A. R.; Schaffner, K. *Photochem. Photobiol.* **1996**, *63*, 92−99.
(21) Amakawa, M.; Tamiaki, H. *Bioorg. Med. Chem.* **1999**, *7*, 1141−1144.
(22) Miyatake, T.; Tamiaki, H.; Holzwarth, A. R.; Schaffner, K. *Photochem. Photobiol.* **1999**, *69*, 448−456.
(23) Metz, G.; Wu, X. L.; Smith, S. O. *J. Magn. Reson. Ser. A* **1994**, *110*, 219−227.
(24) Bennett, A. E.; Rienstra, C. M.; Auger, M.; Lakshmi, K. V.; Griffin, R. G. *J. Chem. Phys.* **1995**, *103*, 6951−6958.
(25) Bennett, A. E.; Ok, J. H.; Griffin, R. G.; Vega, S. *J. Chem. Phys.* **1992**, *96*, 8624−8627.
(26) Ackerman, J. J. H.; Orr, T. V.; Bartuska, V. J.; Maciel, G. E. *J. Am. Chem. Soc.* **1979**, *101*, 341.
(27) Herzfeld, J.; Berger, A. E. *J. Chem. Phys.* **1980**, *73*, 6021−6030.
(28) Eichele, K.; Wasylishen, R. E. *HBA*, version 1.4; Dalhousie University: Halifax, Nova Scotia, Canada, 2001.
(29) de Boer, I.; Bosman, L.; Raap, J.; Oschkinat, H.; de Groot, H. J. M. *J. Magn. Reson.* **2002**, *157*, 286−291.
(30) Abraham, R. J.; Rowan, A. E. Nuclear magnetic resonance spectroscopy of chlorophyll. In *Chlorophylls*; Scheer, H., Ed.; CRC Press: Boca Raton, FL, 1991; pp 797−834.
(31) Vinogradov, E.; Madhu, P. K.; Vega, S. *Chem. Phys. Lett.* **1999**, *314*, 443−450.
(32) Mulder, F. M.; Heinen, W.; van Duin, M.; Lugtenburg, J.; de Groot, H. J. M. *J. Am. Chem. Soc.* **1998**, *120*, 12891−12894.
(33) Wilhelm, M.; Feng, H.; Tracht, U.; Spiess, H. W. *J. Magn. Reson.* **1998**, *134*, 255−260.
(34) Lange, A.; Luca, S.; Baldus, M. *J. Am. Chem. Soc.* **2002**, *124*, 9704−9705.
(35) Yagai, S.; Miyatake, T.; Shimono, Y.; Tamiaki, H. *Photochem. Photobiol.* **2001**, *73*, 153−163.
(36) Anderson, W. P.; Edwards, W. D.; Zerner, M. C. *Inorg. Chem.* **1986**, *25*, 2728−2732.
(37) Wang, Z. Y.; Umetsu, M.; Kobayashi, M.; Nozawa, T. *J. Am. Chem. Soc.* **1999**, *121*, 9363−9369.
(38) Boxer, S. G.; Closs, G. L.; Katz, J. J. *J. Am. Chem. Soc.* **1974**, *96*, 7058−7066.
(39) de Boer, I.; Bosman, L.; Raap, J.; Oschkinat, H.; de Groot, H. J. M. *J. Magn. Reson.* **2002**, *157*, 286−291.
(40) de Boer, I.; Matysik, J.; Amakawa, M.; Yagai, S.; Tamiaki, H.; Holzwarth, A. R.; de Groot, H. J. M. *J. Am. Chem. Soc.* **2003**, *125*, 13374−13375.
(41) Staehelin, L. A.; Golecki, J. R.; Fuller, R. C.; Drews, G. *Arch. Mikrobiol.* **1978**, *119*, 269−277.

(42) Prokhorenko, V. I.; Steensgaard, D. B.; Holzwarth, A. F. *Biophys. J.* **2000**, *79*, 2105−2120.

(43) van Rossum, B. J.; Schulten, E. A. M.; Raap, J.; Oschkinat, H.; de Groot, H. J. M. *J. Magn. Reson.* **2002**, *155*, 1−14.

(44) Umetsu, M.; Hollander, J.; Wang, Z. Y.; Nozawa, T.; de Groot, H. J. M. *J. Phys. Chem. B* **2004**, *108*, 2726−2734.

(45) Tamiaki, H.; Takeuchi, S.; Tsudzuki, S.; Miyatake, T.; Tanikaga, R. *Tetrahedron* **1998**, *54*, 6699−6718.

(46) Tamiaki, H.; Kubo, M.; Oba, T. *Tetrahedron* **2000**, *56*, 6245−6257.

(47) Miyatake, T.; Oba, T.; Tamiaki, H. *ChemBioChem* **2001**, *2*, 335−342.

(48) Saga, Y.; Matsuura, K.; Tamiaki, H. *Photochem. Photobiol.* **2001**, *74*, 72−80.

(49) Sasaki, S.; Omoda, M.; Tamiaki, H. *J. Photochem. Photobiol. A: Chem.* **2004**, *162*, 307−315.

(50) Sasaki, S.; Tamiaki, H. *Bull. Chem. Soc. Jpn.* **2004**, *77*, 797−800.

(51) Tamiaki, H.; Kitamoto, H.; Nishikawa, A.; Hibino, T.; Shibata, R. *Bioorg. Med. Chem.* **2004**, *12*, 1657−1666.

(52) Mizoguchi, T.; Saga, Y.; Tamiaki, H. *Photochem. Photobiol. Sci.* **2002**, *1*, 780−787.

(53) Kunieda, M.; Mizoguchi, T.; Tamiaki, H. *Photochem. Photobiol.* **2004**, *79*, 55−61.

(54) Balaban, T. S.; Holzwarth, A. R.; Schaffner, K. *J. Mol. Struct.* **1995**, *349*, 183−186.

(55) Chiefari, J.; Griebenow, K.; Griebenow, N.; Balaban, T. S.; Holzwarth, A. R.; Schaffner, K. *J. Phys. Chem.* **1995**, *99*, 16194−16194.

(56) Tamiaki, H.; Takeuchi, S.; Tanikaga, R.; Balaban, S. T.; Holzwarth, A. R.; Schaffner, K. *Chem. Lett.* **1994**, 401−402.